RSC Advances

PAPER

View Article Online
View Journal | View Issue



Cite this: *RSC Adv.*, 2023, **13**, 8779

# Dimerized fusion inhibitor peptides targeting the HR1–HR2 interaction of SARS-CoV-2†

Kohei Tsuji, ‡*[a] Kofi Baffour-Awuah Owusu,‡[a] Yutaro Miura,[a] Takahiro Ishii,[a] Kouki Shinohara,[a] Takuya Kobayakawa, [a] Akino Emi,[b] Takashi Nakano,[b] Youichi Suzuki[b] and Hirokazu Tamamura *[a]

Received 19th November 2022
Accepted 27th February 2023

DOI: 10.1039/d2ra07356k

rsc.li/rsc-advances

Membrane fusion is a critical and indispensable step in the replication cycles of viruses such as SARS-CoV-2 and human immunodeficiency virus type-1 (HIV-1). In this step, a trimer of the heptad repeat 1 (HR1) region interacts with the three HR2 regions and forms a 6-helix bundle (6-HB) structure to proceed with membrane fusion of the virus envelope and host cells. Recently, several researchers have developed potent peptidic SARS-CoV-2 fusion inhibitors based on the HR2 sequence and including some modifications. We have developed highly potent HIV-1 fusion inhibitors by dimerization of its HR2 peptides. Here, we report the development of dimerized HR2 peptides of SARS-CoV-2, which showed significantly higher antiviral activity than the corresponding monomers, suggesting that the dimerization strategy can facilitate the design of potent inhibitors of SARS-CoV-2.



## Introduction

The pandemic of the novel COVID-19, which is caused by a positive-strand RNA virus SARS-CoV-2, continued in 2022. By July 2022, more than 560 million people had been infected with SARS-CoV-2 and more than 6 million people had died of the virus-induced disease. To date, more than 30 vaccines have been approved and clinically used worldwide to prevent SARS-CoV-2 infection and COVID-19 aggravation.[1] Some drugs have been developed and authorized in many countries. These include Remdesivir, a repositioning inhibitor of RNA-dependent RNA polymerase (RdRp) from Ebola hemorrhagic fever, Molnupiravir, a novel SARS-CoV-2 RdRp targeting inhibitor, and Nirmatrelvir, aka Paxlovid, an inhibitor of the main protease ($M^{pro}$) of SARS-CoV-2.[2–7] In order to develop drugs with different mechanisms of action and increase the repertory of drug choice, we have focused on fusion inhibitors which inhibit the interaction between heptad repeat 1 (HR1) and HR2, which plays an important role in a membrane fusion step.[8,9] In the entry of SARS-CoV-2 into host cells, a spike protein, S1, on the viral surface binds to its receptor, angiotensin-converting enzyme 2 (ACE2), on the host cell surface (Fig. 1a). The S1 units of the host cell-attached viral particles are cleaved by exogeneous and membrane bound proteases such as trypsin and transmembrane protease, serine 2 (TMPRSS2), or cleaved by lysosomal protease such as cathepsin L after endocytosis. The resulting fusion peptides at N-termini of the S2 units are inserted into the host cell membrane (Fig. 1b). Then three HR2 regions interact with trimer of HR1 regions, and this complex forms a 6-helix bundle (6HB). This facilitates proceeding the membrane fusion of the viruses and the host cells.

Recently, there have been many reports of development of fusion inhibitors based on the SARS-CoV-2 HR2 region, including the HR2 region peptide itself and its stapled peptides,[10–13] and EK1, which was derived from the HR2 region of an α-coronavirus strain HCoV-OC43 and its C-terminally lipidated peptides.[14,15] It is also reported that the HR2 region in the S2 unit is highly conserved among the existing mutants of SARS-CoV-2 from the alpha strain to the omicron strain (B.1.1.529).[16] There is only one mutation (K1191N) of the HR2 region in the alpha strain. On the other hand, mutations of the S1 unit especially for the receptor binding domain (RBD) are frequently observed. Therefore, it seems to be difficult to develop universal anti-SARS-CoV-2 agents targeting the S1 unit. In fact, some of the developed neutralizing monoclonal antibodies dramatically decrease their potencies against the recent variants compared to that against the ancestral Wuhan strain.[17–19] Therefore, it would be worth developing fusion inhibitors as universal anti-SARS-CoV-2 agents.

According to the virus classifications, human immunodeficiency virus type-1 (HIV-1) and SARS-CoV-2 both are positive-

[a]*Department of Medicinal Chemistry, Institute of Biomaterials and Bioengineering, Tokyo Medical and Dental University (TMDU), Chiyoda-ku, Tokyo 101-0062, Japan. E-mail: ktsuji.mr@tmd.ac.jp; tamamura.mr@tmd.ac.jp; Tel: +81-3-5280-8038; +81-3-5280-8036*

[b]*Department of Microbiology and Infection Control, Faculty of Medicine, Osaka Medical and Pharmaceutical University, Takatsuki, Osaka 569-8686, Japan*

† Electronic supplementary information (ESI) available: General information, details of synthesis of the compounds, characterization data of the compounds including MS and analytical HPLC charts to check the purity of the compounds, and data of their biological evaluation. See DOI: https://doi.org/10.1039/d2ra07356k

‡ These authors contributed equally to this study.

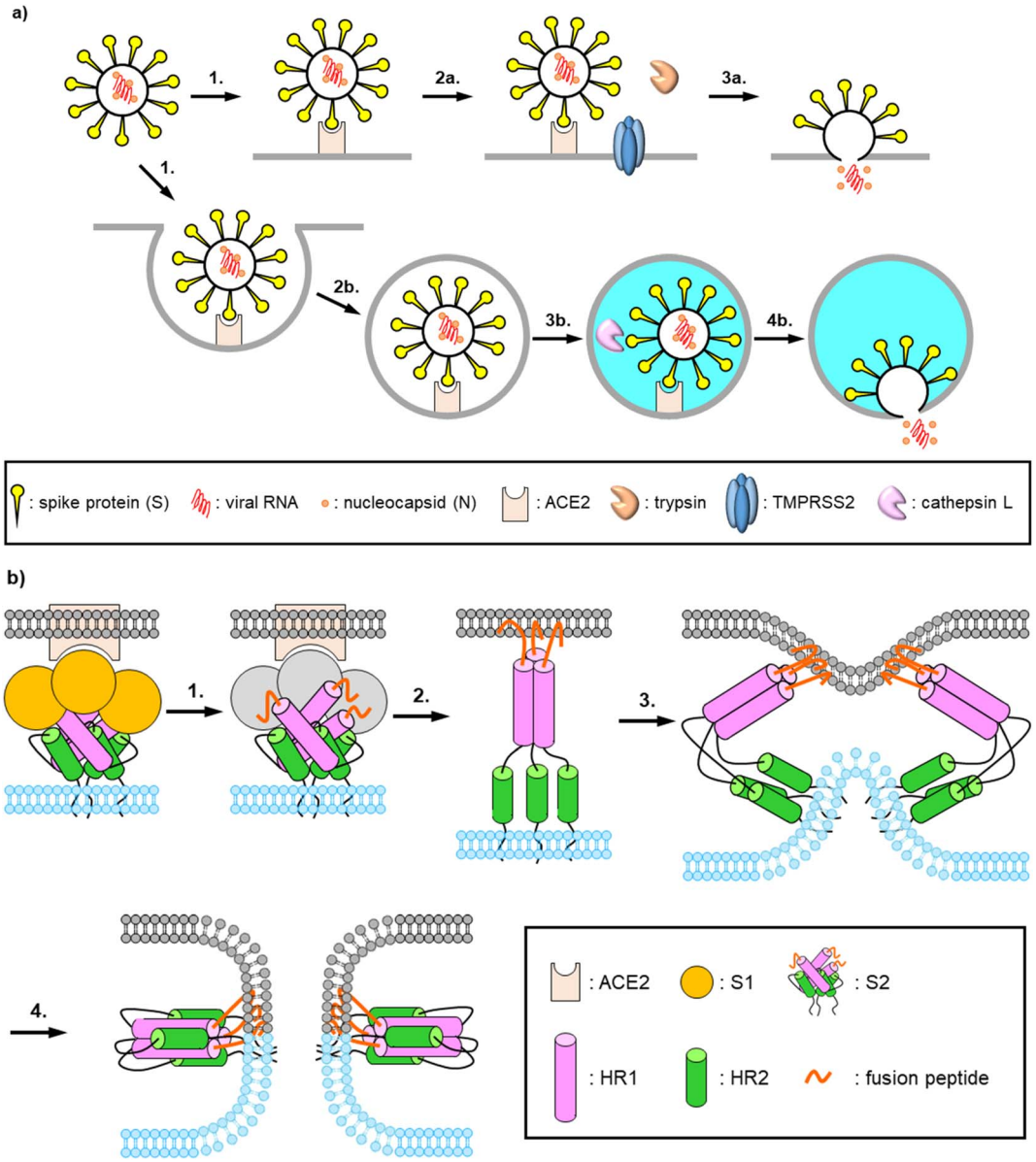


Fig. 1 Schematic representations of entry and fusion mechanisms of SARS-CoV-2. (a) Dual entry pathway of SARS-CoV-2 infection: (1) binding of spike proteins on the virus surface to the receptor, ACE2, on the host cell surface; (2a) processing of the S1 units by exogeneous and membrane bound proteases; (3a) membrane fusion and releasing viral RNA; (2b) internalization *via* endocytosis; (3b) endosomal acidification and processing of the S1 units by lysosomal proteases; (4b) membrane fusion and releasing virus RNA. (b) Membrane fusion mechanism of SARS-CoV-2: (1) receptor binding and processing of the S1 units by host proteases; (2) insertion of the exposed fusion peptides into the host cell membrane; (3) comformational changes of the S2 units with viral and host cell membrane approach; (4) formig 6-helix bundles and membrane fusion.

sense, single-stranded RNA viruses. These viruses have a similar fusion mechanism which includes the formation of 6-HB by interaction of a trimer of HR1 regions with three corresponding HR2 regions (Fig. 2a).[8,9,15,20–23] In the past two decades, we have been developing anti-HIV-1 agents including fusion inhibitors,[24–28] and have found that the C-terminal dimer of HIV-1 HR2 region (C34) based peptides demonstrated two orders of magnitude higher potency than the parent monomeric peptides (Fig. 2b).[26,27] Consequently, we envisioned that this dimerization strategy can be applicable to the development of novel SARS-CoV-2 fusion inhibitors.

## Results and discussion

### Design of fusion inhibitors

From a reported crystal structure of SARS-CoV-2 HR1–HR2, which leads to 6-HB (PDB code: 6LXT, Fig. 3),[15] we extracted a 34-mer HR2 fragment (1169I–1202E) (**1**) as an initial sequence for the design of an inhibitor. A peptide correlated with **1**,

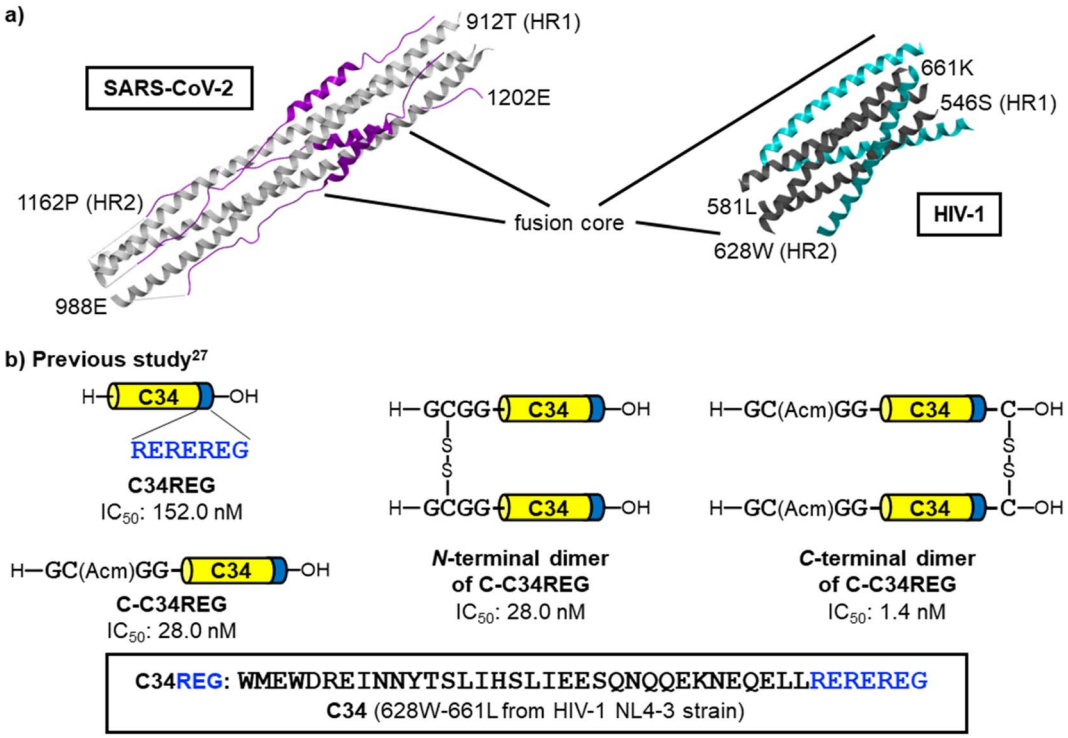


Fig. 2 Representation of the 6-helix bundle (6-HB) structures of SARS-CoV-2 and HIV-1 and the dimerized fusion inhibitors of HIV-1. (a) The SARS-CoV-2 HR1–HR2 crystal structure forming 6-HB (left, PDB code: 6LXT, white: HR1, purple: HR2) and the crystal structure of HIV-1 gp41 HR1 fragment N36 and HR2-derived fusion inhibitor SC34EK[24] forming 6-HB (right, PDB code: 2Z2T, dark gray: HR1, cyan: HR2). (b) Our previous findings in the HIV-1 research;[27] dimerization of HR2-derived peptides resulted highly potent fusion inhibitors. The dimerization at the C-terminus is preferable to that at the N-terminus.

(1168D–1203L, a 36-mer), showed significant anti-SARS-CoV-2 activity in plaque reduction assays using the SARS-CoV-2 ancestral Wuhan strain/VeroE6 cells.[12] Since SARS-CoV, which was reported in 2002 to cause severe acute respiratory syndrome (SARS),[29,30] has an HR2 amino acid sequence identical with that of SARS-CoV-2,[14,15] we also focused on a 35-mer peptide,

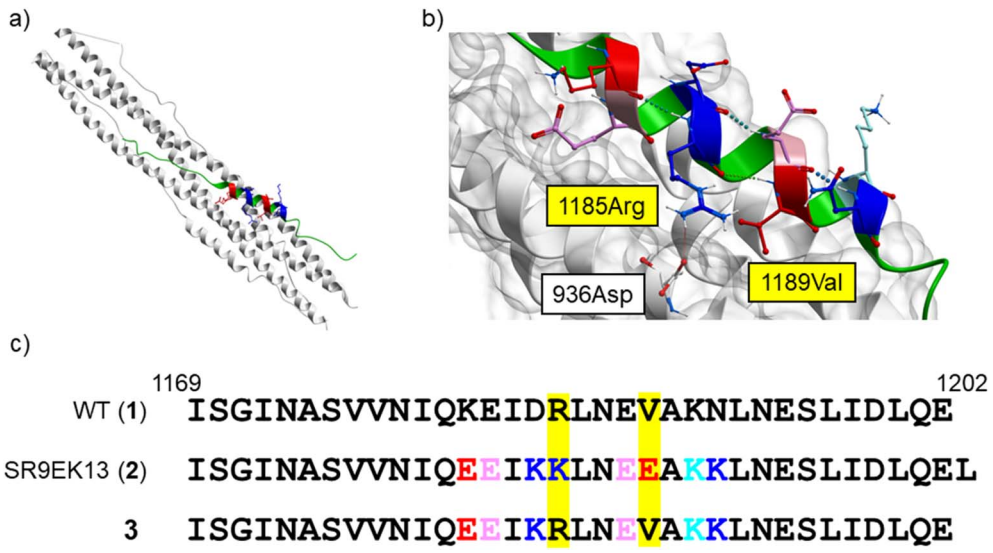


Fig. 3 (a) The SARS-CoV-2 HR1–HR2 crystal structure forming 6-HB (PDB code: 6LXT).[15] (b) A focused structure around 1185Arg and 1189Val of the HR2 region. A hydrogen bond between 1185Arg (in HR2) and 936Asp (in HR1) is observed. HR1 region: white ribbon with grey surface; HR2 region: green, pink (Glu), red (mutated to Glu in SR9EK13 (**2**)), light blue (Lys), and blue (mutated to Lys in SR9EK13 (**2**)). (c) The sequences of SARS-CoV-2 HR2 (1169I–1202E) (**1**), SR9EK13, described with the corresponding position alignment (**2**) and its modified sequence (**3**).

SR9EK13 (**2**), which has been reported as a fusion inhibitor of SARS-CoV (Fig. 3).[31] SR9EK13 (**2**) has 4 pairs of Glu (position *i*)-Lys (*i* + 3 position). Placement of Glu at the *i* position and Lys at the *i* + 3 or *i* + 4 position causes formation of a salt bridge between their sidechains, leading to a significant increase of α-helicity and aqueous solubility.[24] According to the crystal structure of SARS-CoV-2 HR1–HR2, which forms 6-HB (PDB code: 6LXT, Fig. 3), 1185Arg and 1189Val of the HR2 region interact with the HR1 region. Therefore, an SR9EK13-modified 34-mer derivative, in which Lys17 and Glu21 were converted to wild type amino acids Arg and Val, respectively, with deletion of the C-terminal residue Leu35 (**3**), was considered. Based on these sequences, several monomeric peptides were designed.

### Design of monomeric peptides

For the molecular design, all of the monomeric peptides were modified by N-terminal acetylation and C-terminal carboxyamidation. First, a peptide with the above 34-mer HR2 fragment (1169I–1202E) sequence (**1a**) was designed (Fig. 4). The HR2 region might have low aqueous solubility because of its hydrophobic region,[11] and a hydrophilic tag sequence[32] (RERERE)-attached HR2 peptide derivative (**1b**) was designed. As in the 34-mer HR2 fragment (**1**), the C-terminal residue Leu35 of a 35-mer peptide SR9EK13 (**2**) was deleted and its 34-mer derivative (**2a**) was designed. Derivative **3a**, which corresponds to sequence **3**, was also developed. Peptide **2a** has 4 Glu–Lys pairs, and **3a** has 2 such pairs. In addition, introduction of Glu–Lys pairs into peptide **1a** was examined. Peptide **4a** has 2 Glu–Lys pairs in positions 16–20 and 24–27 and **5a** has these in positions 10–13 and 16–20. Peptide **6a** possesses 3 Glu–Lys pairs in positions 10–13, 16–20 and 24–27, which includes the above Glu–Lys pairs of peptides **4a** and **5a**. Peptide **7a** has the 2 reverse pairs: Lys–Glu in positions 13–16 and 20–24. Peptide **8a** is an HCoV-OC43 HR2-derived peptide EK1, which has been reported as a pan-coronavirus fusion inhibitor peptide.[14,15]

### Design of octa-arginine-conjugated monomers

The addition of a cell-penetrating octa-arginyl moiety[33] was attempted. Because our antiviral assay system uses TMPRSS2-expressing VeroE6 cells which allow viruses to enter *via* a cell surface route,[34,35] cell membrane permeability might not be necessary, but the following peptides were designed to confirm their activity and increase aqueous solubility. Peptide **1c** has an octa-arginyl group on the sidechain thiol group of the C-terminal Cys residue through a $G_3SG_3$-C linker attached to the C-terminus of peptide **1a** (Fig. 5). Peptide **1d** has an octa-arginyl group at the C-terminus through a GSG-$(miniPEG)_2$ linker attached to peptide **1a**. Peptide **1e** has an octa-arginyl group on

**1a** Ac–**ISGINASVVNIQKEIDRLNEVAKNLNESLIDLQE**–$NH_2$

**1b** Ac–**ISGINASVVNIQKEIDRLNEVAKNLNESLIDLQE–RERERE–GC**($CH_2CONH_2$)–$NH_2$

**2a** Ac–**ISGINASVVNIQEEIKKLNEEAKKLNESLIDLQE**–$NH_2$

**3a** Ac–**ISGINASVVNIQEEIKRLNEVAKKLNESLIDLQE**–$NH_2$

**4a** Ac–**ISGINASVVNIQKEIERLNKVAKELNKSLIDLQE**–$NH_2$

**5a** Ac–**ISGINASVVEIQKEIERLNKVAKNLNESLIDLQE**–$NH_2$

**6a** Ac–**ISGINASVVEIQKEIERLNKVAKELNKSLIDLQE**–$NH_2$

**7a** Ac–**ISGINASVVNIQKEIERLNKVAKELNESLIDLQE**–$NH_2$

**8a** Ac–**SLDQINVTFLDLEYEMKKLEEAIKKLEESYIDLKEL–GSGK**(Ac)–$NH_2$

Fig. 4 Structures of designed monomeric peptides. E (red), K (blue): mutation introduction; E (pink), K (light blue): natural sequence; placement of E (*i* position) and K (*i* + 3 or *i* + 4 position) or placement of K (*i* position) and E (*i* + 3 or *i* + 4 position) leads to a salt bridge formation between their sidechains.

**1c** Ac–**ISGINASVVNIQKEIDRLNEVAKNLNESLIDLQE–GGGSGGG–C**($CH_2CONH_2$)–$\mathbf{R}_8$–$NH_2$

**1d** Ac–**ISGINASVVNIQKEIDRLNEVAKNLNESLIDLQE–GSG**–$(miniPEG)_2$–$\mathbf{R}_8$–$NH_2$

**1e** Ac–**GC**(Acm)**GG–ISGINASVVNIQKEIDRLNEVAKNLNESLIDLQE–RERERE–GC**($CH_2CO$–$\mathbf{R}_8$–$NH_2$)–$NH_2$

**2b** Ac–**ISGINASVVNIQEEIKKLNEEAKKLNESLIDLQE–GGGSGGG–C**($CH_2CONH_2$)–$\mathbf{R}_8$–$NH_2$

**3b** Ac–**ISGINASVVNIQEEIKRLNEVAKKLNESLIDLQE–GGGSGGG–C**($CH_2CONH_2$)–$\mathbf{R}_8$–$NH_2$

**4b** Ac–**ISGINASVVNIQKEIERLNKVAKELNKSLIDLQE–GGGSGGG–C**($CH_2CONH_2$)–$\mathbf{R}_8$–$NH_2$

**5b** Ac–**ISGINASVVEIQKEIERLNKVAKNLNESLIDLQE–GGGSGGG–C**($CH_2CONH_2$)–$\mathbf{R}_8$–$NH_2$

**6b** Ac–**ISGINASVVEIQKEIERLNKVAKELNKSLIDLQE–GGGSGGG–C**($CH_2CONH_2$)–$\mathbf{R}_8$–$NH_2$

**7b** Ac–**ISGINASVVNIQKEIERLNKVAKELNESLIDLQE–GGGSGGG–C**($CH_2CONH_2$)–$\mathbf{R}_8$–$NH_2$

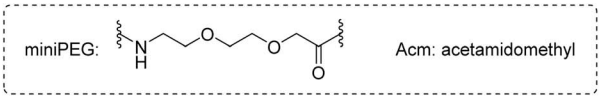


Fig. 5 Structures of octa-arginine ($R_8$)-conjugated peptides.

the sidechain thiol group of the C-terminal Cys residue through an RERERE-GC linker and a GC(Acm)GG sequence attached to peptide **1a**. Peptides **2b**, **3b**, **4b**, **5b**, **6b** and **7b** have an octa-arginyl group on the sidechain thiol group of the C-terminal Cys residue through a $G_3SG_3$-C linker attached to the corresponding peptides **2a**, **3a**, **4a**, **5a**, **6a** and **7a**, respectively, are similar to peptide **1c**.

### Design of C-terminal dimers

Several dimeric derivatives of these monomeric peptides linked through a disulfide bridge at the C-terminus were constructed (Fig. 6). Dimers **1Ca** and **1Cb** are C-terminal disulfide dimers of peptide **1a** with $G_3SG_3$-C and RERERE-GC linkers at the C-terminus, respectively. Dimer **1Cc** is a C-terminal disulfide dimer of peptide **1a** with an additional GC(Acm)GG sequence at the N-terminus and an RERERE-GC linker at the C-terminus. Dimers **2Ca**, **2Cb** and **2Cc** are C-terminal disulfide dimers of peptide **2a** with $G_3SG_3$-C, $G_3SG_3$-C-$R_4$ and $G_3SG_3$-C-$R_8$ linkers at the C-terminus, respectively. Dimers **3C**, **4C**, **5C**, **6C** and **7C** are C-terminal disulfide dimers of peptides **3a**, **4a**, **5a**, **6a** and **7a**, respectively with a $G_3SG_3$-C linker at the C-terminus. Dimer **8C** is a C-terminal disulfide dimer of peptide **8a** built through two Cys residues on the sidechain of the C-terminal Lys residue.

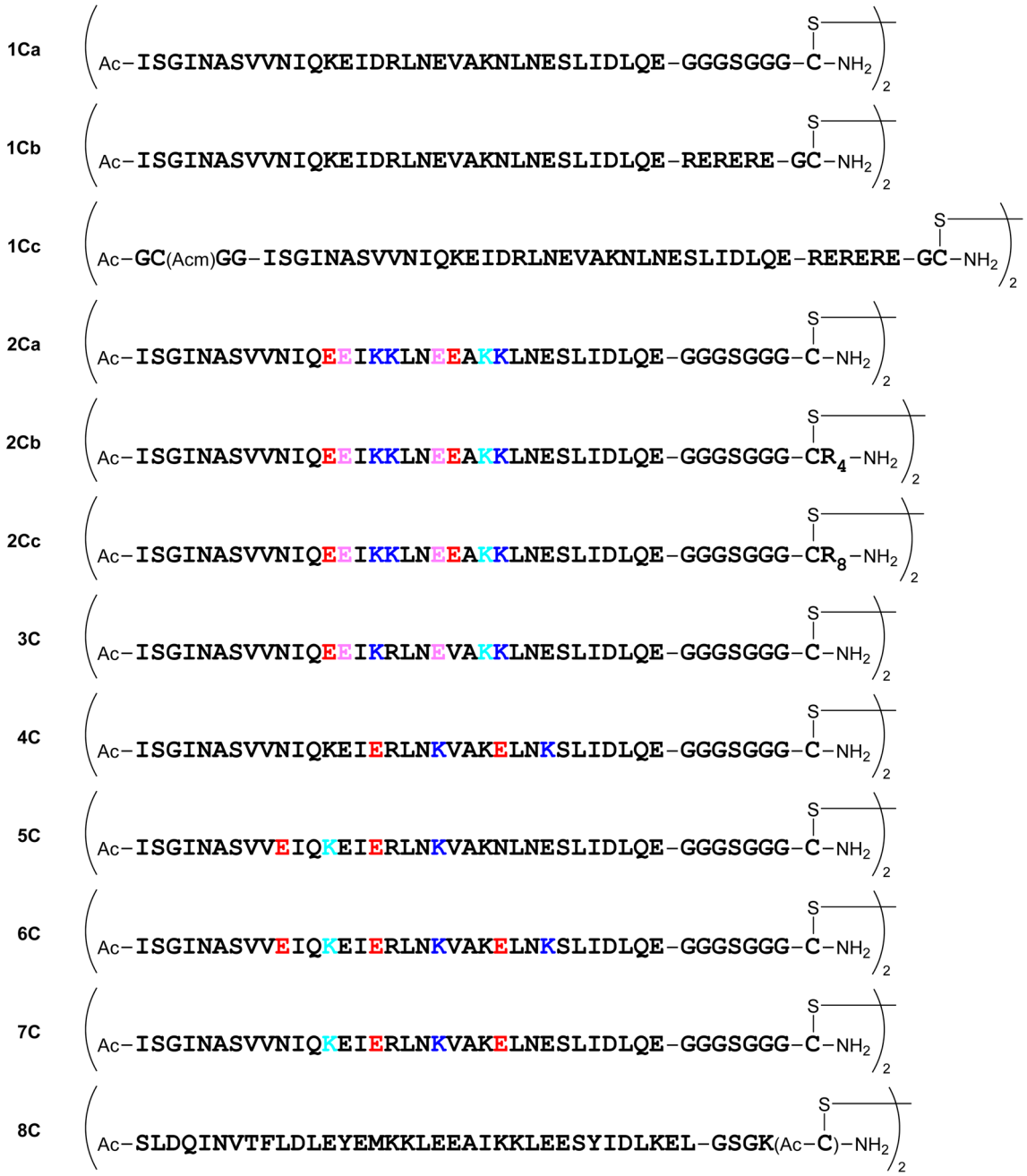


Fig. 6 Structures of C-terminal dimers.


Fig. 7 Structures of N-terminal dimers.

### Design of N-terminal dimers

Several dimeric derivatives of the monomeric peptides linked through a disulfide bridge at the N-terminus were designed (Fig. 7). Dimers **1N**, **2N**, **3N**, **6N** and **7N** are N-terminal disulfide dimers of peptides **1a**, **2a**, **3a**, **6a** and **7a**, respectively with a C-aminohexanoic acid (Ahx) linker at the N-terminus. Dimers **4N**, **5N** and **8N** are N-terminal disulfide dimers of peptides **4a**, **5a** and **8a**, respectively with a CGSG linker at the N-terminus.

### Synthesis of compounds

All monomer peptides and intermediate peptides for the dimer peptides were synthesized using 9-fluorenylmethyloxycarbonyl-based solid phase peptide synthesis (Fmoc-SPPS) methods. The protected peptide resins were constructed manually or with an automatic peptide synthesizer followed by acetylation of the N-terminal amino group. Treatment of the peptide resins with TFA cocktails (trifluoroacetic acid (TFA)/triisopropylsilane-(TIPS)/$H_2O$ or TFA/TIPS/$H_2O$/ethanedithiol (EDT)) followed by purification using reverse-phase (RP)-high performance liquid chromatography (HPLC), afforded the corresponding monomers and intermediate peptides (Scheme 1). Several octa-arginine-conjugated peptides were synthesized using native chemical ligation (Scheme 2).[36] All C- and N-terminal dimers were linked *via* disulfide bonds between two Cys sidechain thiols of the corresponding monomer peptides by air oxidation (Schemes 3 and 4).

### Evaluation of anti-SARS-CoV-2 activity

In order to evaluate the anti-SARS-CoV-2 activity of the peptides, a plaque reduction assay[37] using the SARS-CoV-2 ancestral Wuhan strain/VeroE6 cells was performed. The results of the assays are shown in Tables 1–4. Peptide **1a** showed significant antiviral activity (Table 1). Peptide **1b** showed slightly higher antiviral activity than peptide **1a**, indicating the addition of a hydrophilic tag sequence (RERERE) has a positive effect on the increase of aqueous solubility and enhances antiviral activity. Peptide **2a** showed less antiviral activity than peptide **1a**. This suggests that Glu substitution for 1189Val or Lys substitution for 1185Arg is not suitable because 1185Arg and 1189Val of the HR2 region interact with the HR1 region (Fig. 3). Peptide **3a** showed approximately 10 and 4 times higher antiviral activity than peptides **2a** and **1a**, respectively, suggesting that the return changing of Lys17 and Glu21 to wild type amino acids Arg and Val, respectively, is compatible with interaction with the HR1 region. Peptides **4a** and **5a**, which have 2 Glu–Lys pairs, exhibited half of the antiviral activity of peptide **3a**, but both are

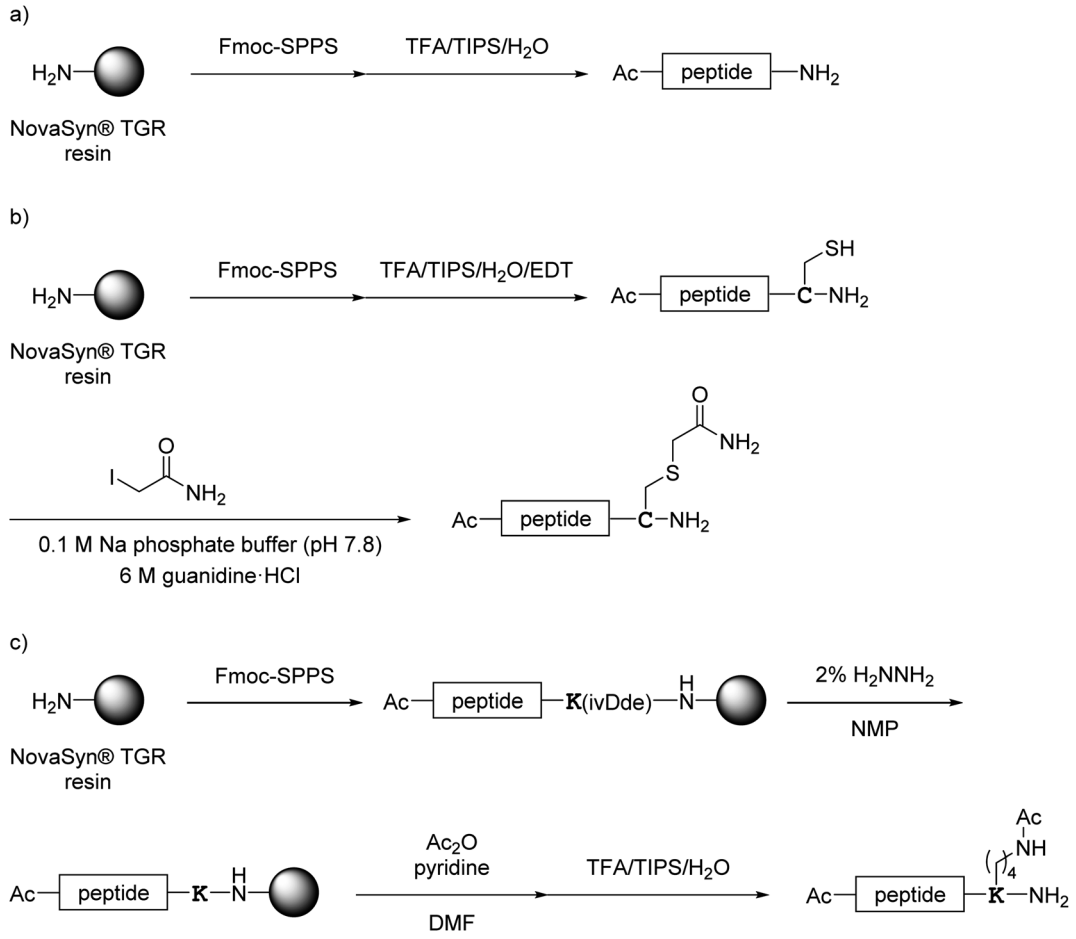


Scheme 1 Synthesis of monomer peptides shown in Fig. 4. (a) Preparation of **1a** and **2a–7a**; (b) preparation of **1b**; (c) preparation of **8a**.

more active than peptide **1a**. Peptide **6a**, which has 3 Glu–Lys pairs, showed remarkably less antiviral activity than peptides **1a**, **4a** and **5a**. This indicates that substitution of 3 Glu–Lys pairs in a wide area at positions 10–13, 16–20 and 24–27 in peptide **6a** is not appropriate because substitution of 2 Glu–Lys pairs at the same positions caused no problems in peptides **4a** and **5a**. Peptide **7a**, which has the 2 reverse pairs: Lys–Glu in positions 13–16 and 20–24, also exhibited remarkably less antiviral activity than peptides **1a**, **4a** and **5a**, suggesting that the introduction of reverse pairs, Lys–Glu, might be unsuitable. Peptide **8a**, which is the HCoV-OC43 HR2-derived peptide, EK1 with significant broad antiviral activity against various corona viruses, exhibited significant but slightly diminished antiviral activity compared to peptide **1a**. This result is consistent with previous reports from the other research groups.[14]

Peptide **1c**, which has an octa-arginyl group on the sidechain thiol group of the C-terminal Cys residue through a $G_3SG_3$-C linker attached to peptide **1a**, showed less antiviral activity than peptide **1a**, indicating that the addition of an octa-arginyl group at the C-terminus through a $G_3SG_3$-C linker has no positive effects on antiviral activity, and that nonspecific interaction of its octa-arginyl group might reduce affinity for the HR1 region (Table 2). Peptide **1d**, which has an octa-arginyl group at the C-terminus through a GSG-$(miniPEG)_2$ linker attached to peptide **1a**, showed slightly higher antiviral activity than peptide **1a**. Peptide **1e**, which has an octa-arginyl group on the sidechain thiol group of the C-terminal Cys residue through an RERERE-GC linker attached to peptide **1a**, exhibited twice the antiviral activity of peptide **1a**, suggesting that the addition of an octa-arginyl group at the C-terminus through a GSG-$(miniPEG)_2$ or RERERE-GC linker might not be responsible for its nonspecific interaction. Peptides **2b** and **6b**, which have an octa-arginyl group at the C-terminus through a $G_3SG_3$-C linker attached to peptides **2a** and **6a**, showed remarkably increased potency compared to peptides **2a** and **6a**, respectively, whereas peptides **3b**, **4b**, **5b** and **7b**, which have an octa-arginyl group at the C-terminus through a $G_3SG_3$-C linker attached to peptides **3a**, **4a**, **5a** and **7a**, showed decreased or retained the potency compared to peptides **3a**, **4a**, **5a** and **7a**, respectively. As a result, the addition of an octa-arginyl group at the C-terminus through a $G_3SG_3$-C linker might be effective for enhancement of the potency of only low-active parent peptides, but might cause a decrease in the potency of high-activity parent peptides. Enhancement of antiviral activity based on an increase of aqueous solubility due to the addition of an octa-arginyl group was not observed. This suggests that the positive effects of the addition of an octa-arginyl group are limited. Taken together, these data confirm that the addition of an octa-arginyl group for

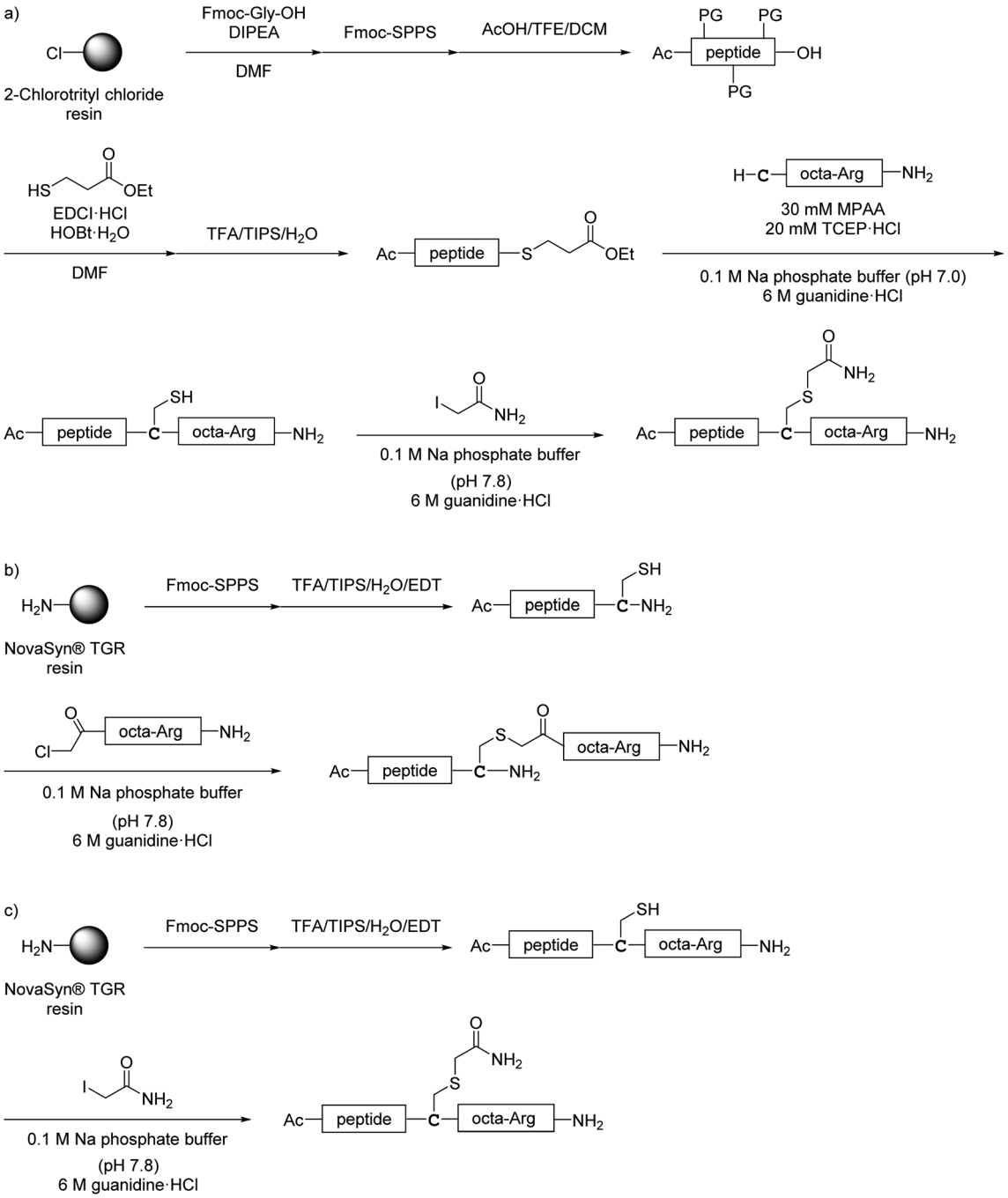


Scheme 2 Synthesis of octa-arginine-conjugated peptides shown in Fig. 5. (a) Preparation of **1c**, **2b**, **3b** and **6b**; (b) preparation of **1e**; (c) preparation of **4b**, **5b** and **7b**. Peptide **1d** was synthesized as shown in Scheme 1a.

the introduction of the peptides into cells is not required because in this assay system, the virus enters cells *via* the TMPRSS2-processing cell surface pathway instead of by an endocytosis pathway.

Dimer **1Ca**, which is a C-terminal disulfide dimer of peptide **1a** with a $G_3SG_3$-C linker at the C-terminus, exhibited slightly higher antiviral activity than the corresponding monomer (**1a**) although dimer **1Ca** has twice the monomer peptide content (Table 3). Dimer **1Cb**, which is a C-terminal disulfide dimer of peptide **1b** at the C-terminus, exhibited slightly less antiviral activity than the corresponding monomer (**1b**) although dimer **1Cb** has twice the monomer peptide content. Dimer **1Cc**, which has an additional GC(Acm)GG sequence at the N-terminus of dimer **1Cb**, showed less antiviral activity than peptide **1Cb**. In terms of peptide contents, there was no advantage for dimerization even when using a linker of $G_3SG_3$-C (**1Ca**) or RERERE-GC (**1Cb**/**1Cc**) at the C-terminus. The additional GC(Acm)GG sequence at the N-terminus in dimer **1Cc** was not appropriate.

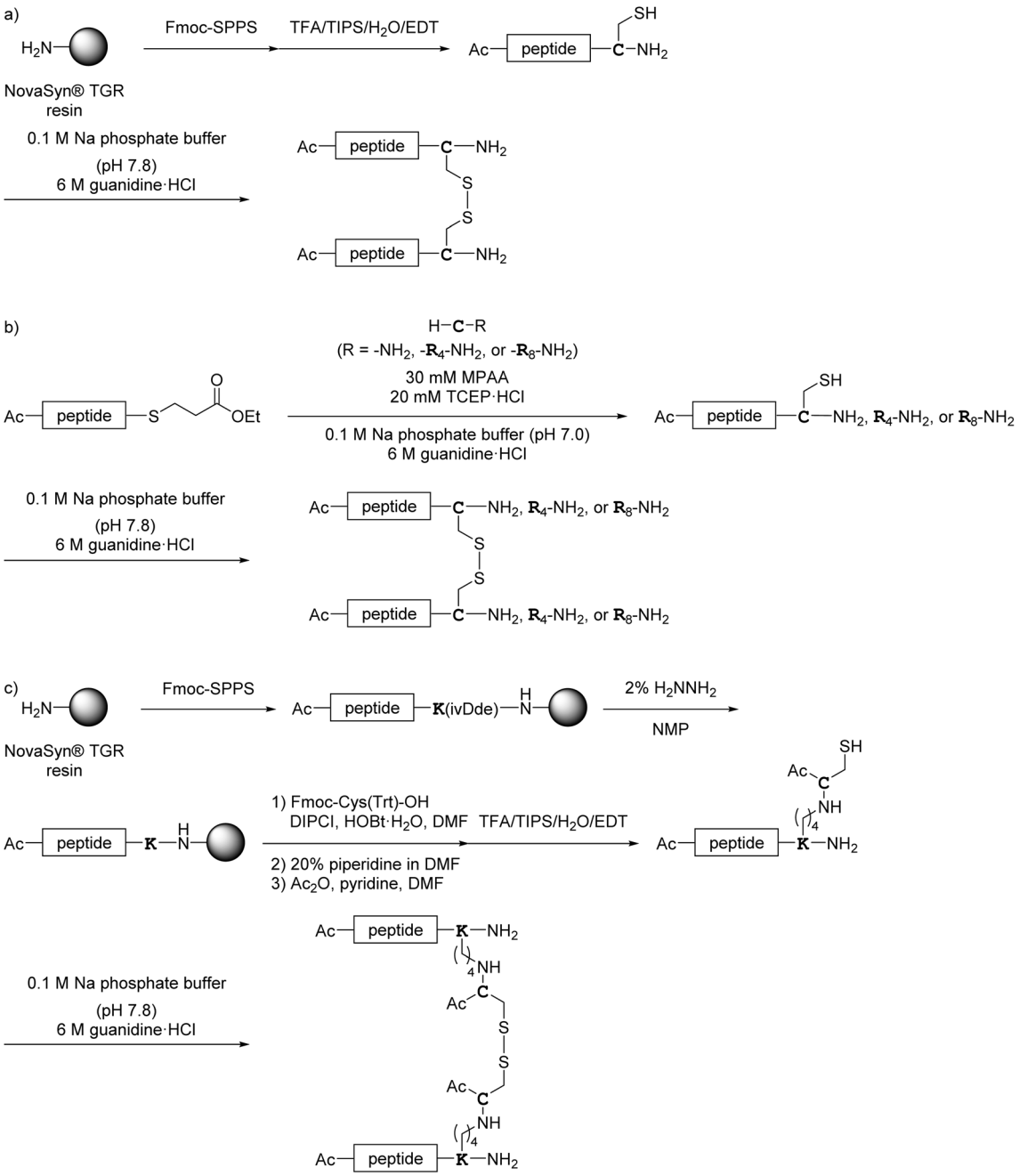


Scheme 3 Synthesis of the C-terminal dimers shown in Fig. 6. (a) Preparation of **1Ca**, **1Cb**, **1Cc**, **4C**, **5C** and **7C**; (b) preparation of **2Ca**, **2Cb**, **2Cc**, **3C** and **6C**; (c) preparation of **8C**.

Dimers **2Ca**, **2Cb** and **2Cc**, which are C-terminal disulfide dimers of peptide **2a** with $G_3SG_3$-C, $G_3SG_3$-C-$R_4$ and $G_3SG_3$-C-$R_8$ linkers at the C-terminus, respectively, showed remarkably higher antiviral activity compared to the corresponding monomer (**2a**), but almost the same level of antiviral activity as peptide **1a**. There is an evident advantage gained by dimerization, but no positive effects were observed for the addition of tetra-arginine/octa-arginine. Dimer **3C**, a C-terminal disulfide dimer of peptide **3a** with a $G_3SG_3$-C linker at the C-terminus, showed almost the same antiviral activity as the corresponding monomer (**3a**), in which the fold change to the corresponding monomer was calculated from two independent experiments in Table 3. However, **3C** also clearly showed improved antiviral activity from that of the monomer **3a** in the detailed evaluation (Table 5).

Dimers **4C**, **5C**, **6C** and **7C**, which are C-terminal disulfide dimers of peptides **4a**, **5a**, **6a** and **7a**, respectively with a $G_3SG_3$-C linker at the C-terminus, exhibited moderately to remarkably higher antiviral activity when compared to the corresponding monomers (**4a**, **5a**, **6a** and **7a**), respectively, and peptide **1a**.

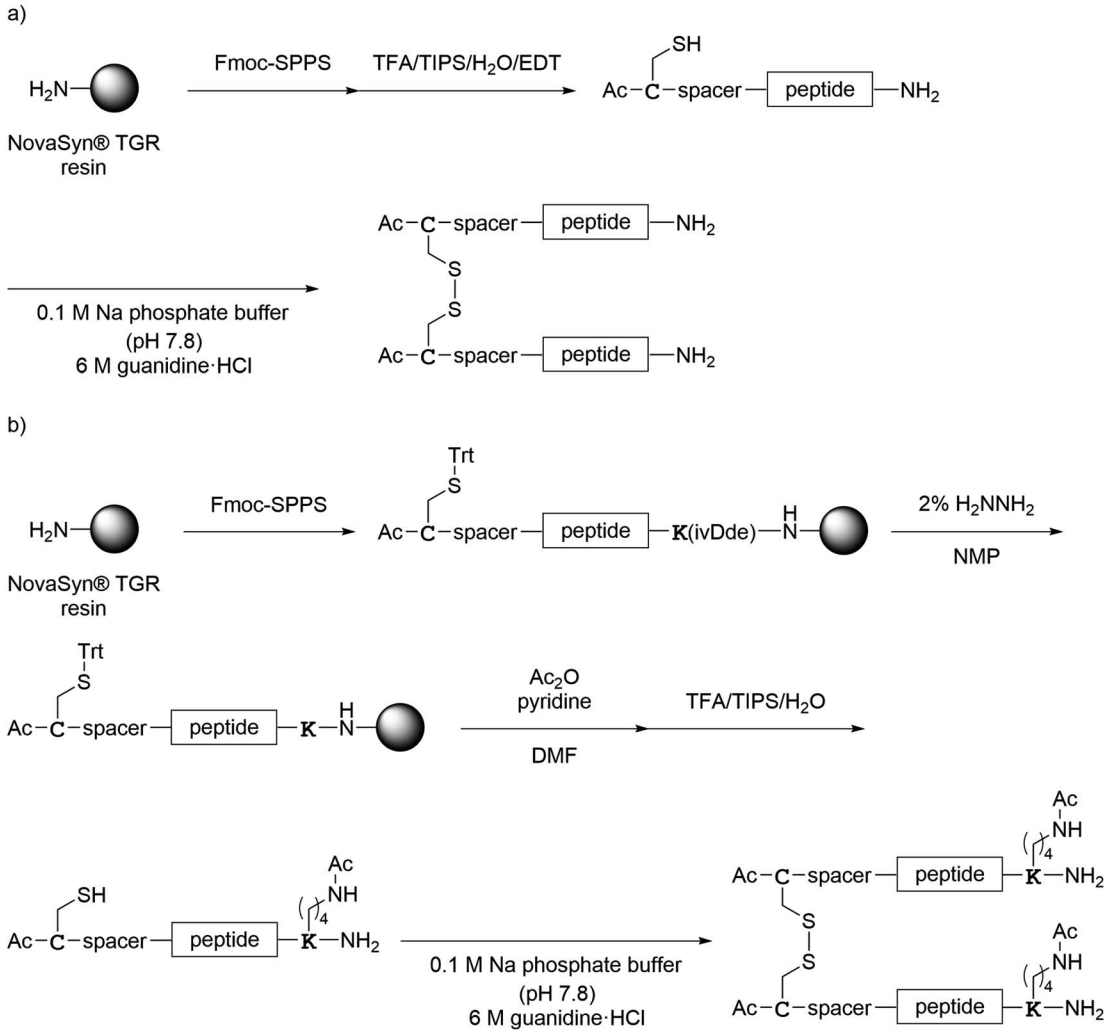


Scheme 4 Synthesis of the N-terminal dimers shown in Fig. 7. (a) Preparation of **1N–7N**; (b) preparation of **8N**.

There is also an obvious advantage for dimerization. Dimer **8C**, which is a C-terminal disulfide dimer of peptide **8a** through two Cys residues on the sidechain of the C-terminal Lys residue, exhibited almost the same antiviral activity as the corresponding monomer (**8a**), but less antiviral activity than peptide **1a**.

All of the dimers (**2Ca**, **3C**, **4C**, **5C**, **6C** and **7C**) have significantly higher antiviral activity than the corresponding monomers (**2a**, **3a**, **4a**, **5a**, **6a** and **7a**), respectively. Dimerized HR2 peptides at the C-termini with introduction of Glu–Lys pairs into peptide **1a** clearly have effectiveness of dimerization

Table 1 Anti-SARS-CoV-2 activity of normal monomeric peptides (**1a**, **1b**, **2a**, **3a**, **4a**, **5a**, **6a**, **7a** and **8a**)

| Peptide | $IC_{50}$ (nM) | Fold change to peptide **1a**[h] |
|---|---|---|
| **1a** | 206 ± 24.5[a], 214[b], 164[c], 155[d], 667[e], 105[f], 2530[g] | 1.00 |
| **1b** | 68.3[f] | 0.648[f] |
| **2a** | 629 ± 59.6[a] | 3.06[a] |
| **3a** | 51.2[b] | 0.240[b] |
| **4a** | 106[d] | 0.683[d] |
| **5a** | 123[d] | 0.793[d] |
| **6a** | 438[c] | 2.68[c] |
| **7a** | 2280[g] | 0.901[g] |
| **8a** | 152[f] | 1.44[f] |

[a] Experiment 1. [b] Experiment 2. [c] Experiment 3. [d] Experiment 4. [e] Experiment 5. [f] Experiment 6. [g] Experiment 7. [h] The values of fold change to peptide **1a** are represented as $IC_{50}^{\text{test compound}}/IC_{50}^{\mathbf{1a}}$ from the same data set.

Table 2 Anti-SARS-CoV-2 activity of octa-arginine-conjugated monomers (**1c**, **1d**, **1e**, **2b**, **3b**, **4b**, **5b**, **6b** and **7b**)

| Peptide | $IC_{50}$ (nM) | Fold change to peptide **1a**[d] |
|---|---|---|
| **1c** | 357[a] | 2.30[a] |
| **1d** | 1150[c] | 0.455[c] |
| **1e** | 50.0[b] | 0.474[b] |
| **2b** | 75.9[b] | 0.720[b] |
| **3b** | 226[a] | 1.46[a] |
| **4b** | 7480[c] | 2.96[c] |
| **5b** | 25 900[c] | 10.2[c] |
| **6b** | 135[b] | 0.868[b] |
| **7b** | 2220[c] | 0.877[c] |

[a] Experiment 4. [b] Experiment 6. [c] Experiment 7. [d] The values of fold change to peptide **1a** are represented as $IC_{50}^{\text{test compound}}/IC_{50}^{\mathbf{1a}}$ from the same data set.

leading to an increase in antiviral activity, although dimers of a wild type including a different corona virus HCoV-OC43 have no significant effectiveness following dimerization.

Dimers **1N**, **2N** and **7N**, which are N-terminal disulfide dimers of peptides **1a**, **2a** and **7a**, respectively with a C-aminohexanoic acid linker at the N-terminus, showed moderately higher antiviral activity than the corresponding monomers (**1a**, **2a** and **7a**), respectively (Table 4). Although slightly positive effects of the dimerization were observed, especially for dimers **2N** and **7N**, these dimers are unsuitable as lead compounds because the antiviral activity of the monomer peptides are relatively low. In addition, peptide contents of the dimers are twice that of the corresponding monomers. Dimers **3N**, **4N**, **5N** and **6N**, which are N-terminal disulfide dimers of peptides **3a**, **4a**, **5a** and **6a**, respectively with a C-aminohexanoic acid linker or a CGSG linker at the N-terminus, showed less or almost the same levels of antiviral activity compared to the corresponding

Table 3 Anti-SARS-CoV-2 activity of C-terminal dimers (**1Ca**, **1Cb**, **1Cc**, **2Ca**, **2Cb**, **2Cc**, **3C**, **4C**, **5C**, **6C**, **7C** and **8C**)

| Peptide | $IC_{50}$ (nM) | Fold change to peptide **1a**[h] | Corresponding monomer ($IC_{50}$ (nM)[i]) | Fold change to the corresponding monomer[j,k] |
|---|---|---|---|---|
| **1Ca** | 1080[g] | 0.427[g] | — | — |
| **1Cb** | 93.3[f] | 0.885[f] | **1b** (68.34[f]) | 1.37[f,j] |
| **1Cc** | 231[f] | 2.19[f] | — | — |
| **2Ca** | 112 ± 9.26[a] | 0.583[a] | **2a** (629 ± 59.6[a]) | 0.191[a,j] |
| **2Cb** | 270 ± 26.2[a] | 1.31[a] | — | — |
| **2Cc** | 286 ± 23.6[a] | 1.39[a] | **2b** (75.9[f]) | 1.93[a,f,k] |
| **3C** | 753[g] | 0.298[g] | **3a** (51.2[b]) | 1.24[b,g,k] |
| **4C** | 155[e] | 0.233[e] | **4a** (106[d]) | 0.341[d,e,k] |
| **5C** | 259[e] | 0.389[e] | **5a** (123[d]) | 0.491[d,e,k] |
| **6C** | 135[d] | 0.868[d] | **6a** (438[c]) | 0.324[c,d,k] |
| **7C** | 213[e] | 0.320[e] | **7a** (2280[g]) | 0.365[e,g,k] |
| **8C** | 252[c] | 1.54[c] | **8a** (152[f]) | 1.07[c,f,k] |

[a] Experiment 1. [b] Experiment 2. [c] Experiment 3. [d] Experiment 4. [e] Experiment 5. [f] Experiment 6. [g] Experiment 7. [h] The values of fold change to peptide **1a** are represented as $IC_{50}^{\text{test compound}}/IC_{50}^{\mathbf{1a}}$ from the same data set. [i] $IC_{50}$ values from Tables 1 and 2. [j] The values of fold change to the corresponding monomer are represented as $IC_{50}^{\text{test compound}}/IC_{50}^{\text{corresponding monomer}}$ from the same data set. [k] The values of fold change to the corresponding monomer are represented as $(IC_{50}^{\text{test compound}}/IC_{50}^{\mathbf{1a}})/(IC_{50}^{\text{corresponding monomer}}/IC_{50}^{\mathbf{1a}})$ from two independent experiments.

Table 4 Anti-SARS-CoV-2 activity of N-terminal dimers (**1N**, **2N**, **3N**, **4N**, **5N**, **6N**, **7N** and **8N**)

| Peptide | $IC_{50}$ (nM) | Fold change to peptide **1a**[g] | Corresponding monomer ($IC_{50}$ (nM)[h]) | Fold change to the corresponding monomer[i,j] |
|---|---|---|---|---|
| **1N** | 35.00[e] | 0.332[e] | **1a** (105[e]) | 0.332[e,i] |
| **2N** | 125 ± 9.78[a] | 0.608[a] | **2a** (629 ± 59.6[a]) | 0.199[a,i] |
| **3N** | 528[b] | 2.47[b] | **3a** (51.2[b]) | 10.3[b,i] |
| **4N** | 267[d] | 1.72[d] | **4a** (106[d]) | 2.52[d,i] |
| **5N** | 155[d] | 0.998[d] | **5a** (123[d]) | 1.26[d,i] |
| **6N** | 459[d] | 2.96[d] | **6a** (438[c]) | 1.10[c,d,j] |
| **7N** | 800[f] | 0.316[f] | **7a** (2280[f]) | 0.351[f,i] |
| **8N** | 41.3[b] | 0.193[b] | **8a** (152[e]) | 0.134[b,e,j] |

[a] Experiment 1. [b] Experiment 2. [c] Experiment 3. [d] Experiment 4. [e] Experiment 6. [f] Experiment 7. [g] The values of fold change to peptide **1a** are represented as $IC_{50}^{\text{test compound}}/IC_{50}^{\mathbf{1a}}$ from the same data set. [h] $IC_{50}$ values from Tables 1 and 2. [i] The values of fold change to the corresponding monomer are represented as $IC_{50}^{\text{test compound}}/IC_{50}^{\text{corresponding monomer}}$ from the same data set. [j] The values of fold change to the corresponding monomer are represented as $(IC_{50}^{\text{test compound}}/IC_{50}^{\mathbf{1a}})/(IC_{50}^{\text{corresponding monomer}}/IC_{50}^{\mathbf{1a}})$ from two independent experiments.

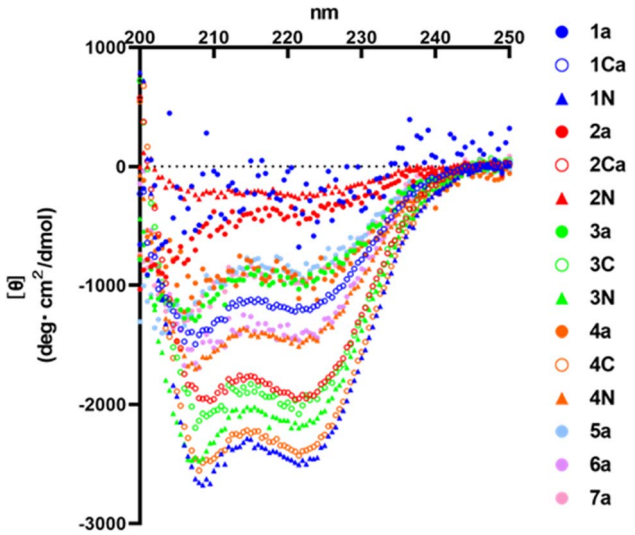


Fig. 8 CD spectra of the HR2 peptides. CD spectra were measured at 25 °C in PBS (50 mM Na phosphate buffer, 150 mM NaCl, pH 7.2).

monomers (**3a**, **4a**, **5a** and **6a**), respectively. Considering the peptide contents of the dimers, the antiviral activities of these dimers are much lower, suggesting that dimerization offers no advantage. Dimer **8N**, which is an N-terminal disulfide dimer of peptide **8a** with a CGSG linker at the N-terminus, exhibited remarkably higher antiviral activity than the corresponding monomer (**8a**).

HR2 peptides dimerized at the N-termini might be unsuitable as lead compounds with the exception of dimer **8N**, which was derived from HCoV-OC43, a different corona virus.

### CD analysis

HR2 is an α-helical region. Therefore, α-helicity of HR2 fragment derivatives might have some effects on inhibitory activity. In this study, circular dichroism (CD) spectra of representative monomer peptides (**1a**, **2a**, **3a**, **4a**, **5a**, **6a** and **7a**), C-terminal dimers (**1Ca**, **2Ca**, **3C** and **4C**) and N-terminal dimers (**1N**, **2N**, **3N** and **4N**) were measured (Fig. 8). It was found that an initial lead monomer peptide (**1a**) or a peptide (**2a**) containing 4 Glu–Lys pairs did not show an α-helical structure. Introduction of Glu–Lys pairs or introduction of 4 pairs did not in any case induce helical formation, suggesting 4 pairs might be excessive. The other monomer peptides (**3a**, **4a**, **5a** and **7a**) showed α-helical structures although their α-helicities were not very high. A 3 Glu–Lys pairs-containing monomer (**6a**) showed an α-helical structure of moderate strength, suggesting that the introduction of 3 Glu–Lys pairs into broad regions might be effective for enhancement of α-helicity. The C-terminal dimer (**1Ca**) exhibited an α-helical structure of moderate strength, and an N-terminal dimer (**1N**) exhibited a remarkably more pronounced α-helical structure than **1Ca**, although the corresponding monomer (**1a**) did not show any α-helical structure. On the contrary, the C-terminal dimer (**4C**) showed a remarkably higher α-helical structure than **4N**, which exhibited a moderately strong α-helical structure, although the corresponding monomer (**4a**) showed a weak α-helical structure. The C-terminal dimer (**2Ca**) showed a relatively high α-helical structure, although the corresponding monomer (**2a**) or its N-terminal dimer (**2N**) failed to show an α-helical structure. The C- and N-terminal dimers (**3C** and **3N**) showed conspicuously high α-helical structures, although the corresponding monomer (**3a**) showed a weak α-helical structure. In general, the α-helicities of the dimers were significantly higher than those of the corresponding monomers. Taken together, introduction of 2 or 3 Glu–Lys pairs and dimerization at the C- or N-terminus generally caused an efficient increase in the α-helicity of the HR2 peptides.

In terms of the antiviral activity, peptide **3a** is the most suitable monomer because it has potent antiviral activity and a weak but clear α-helical structure as a monomer, and amongst the synthesized peptides the C-terminal dimers (**3C** and **4C**) are the most suitable derivatives. According to the previous report, HR2-derived peptides alone did not show α-helical structures, while these peptides showed α-helical structures in the presence of HR1-derived peptide.[11] Therefore, it was considered that the HR2-derived peptides reported here would also form α-helical structures when these peptides bind to the HR1 region of SARS-CoV-2 to show their inhibitory activity.

Table 5 Anti-SARS-CoV-2 activity of the hit peptides (**1a**, **3a**, **3C** and **4C**)[a]

| Peptide | $IC_{50}$ (nM) | Fold change to peptide **1a** |
|---|---|---|
| **1a** | 1700 ± 433 | 1.00 |
| **3a** | 955 ± 194 | 0.563 |
| **3C** | 472 ± 189 | 0.278 |
| **4C** | 575 ± 212 | 0.339 |

[a] The $IC_{50}$ values represent the average $IC_{50}$ value ± SEM (nM) from three independent experiments.

### Detailed evaluation of anti-SARS-CoV-2 activity of the selected peptides

Peptide **3a**, the most suitable monomer, and the C-terminal dimers (**3C** and **4C**), the most suitable derivatives, were statistically analyzed (Table 5). These activities were verified.

## Conclusions

Development of new drugs with different mechanisms of action starting from existing drugs is necessary for increasing the repertory of therapeutic choice. In this study, we focused on and developed fusion inhibitors, which function at the steps of viral entry and fusion into cells. To date, we have developed HIV-1 fusion inhibitors based on dimerization of HR2 region peptides accompanied by introduction of Glu–Lys pairs.[24] Since HIV-1 and SARS-CoV-2 have similar fusion mechanisms involving HR1-HR2 interactions,[8,9,15,20–23] this strategy was applied to the development of inhibitors of SARS-CoV-2. Initially, an HR2 peptide (**1a**) was characterized as an inhibitor with significant antiviral activity against SARS-CoV-2 in

spite the absence of significant α-helicity. Introduction of Glu–Lys pairs into derivatives of HR2 peptides significantly increased the antiviral activity and α-helicity in peptides **3a**, **4a**, **5a** and **7a**. Peptide **3a** was determined to be the most suitable monomer. Effects of the addition of an octa-arginyl group on enhancement of antiviral activity might be limited for original peptides with low potency. There were no positive effects on original peptides with relatively high potency. Since an ancestral Wuhan strain of SARS-CoV-2 enters VeroE6 cells *via* the TMPRSS2-processing cell surface pathway instead of the endocytosis pathway in this assay system, the addition of an octa-arginyl group for the penetration of the peptides into cells is not required. However, it was recently reported that the SARS-CoV-2 omicron (B.1.529) strain prefers infection *via* an endosomal route rather than a cell surface route.[38] Therefore, peptides modified with an octa-arginyl group might be useful for inhibition against universal strains of SARS-CoV-2.

HR2 peptides dimerized at the C-termini with introduction of Glu–Lys pairs into peptide **1a** show the clear effectiveness of dimerization with an increase in antiviral activity. This phenomenon was observed in all of the dimers (**2Ca**, **3C**, **4C**, **5C**, **6C** and **7C**), although dimers of a wild type including a different corona virus HCoV-OC43 showed no significant effectiveness of dimerization. Dimerized HR2 peptides at the N-termini might be unsuitable as lead compounds with the exception of dimer **8N** derived from a different corona virus HCoV-OC43. In CD analysis, dimerization at the C- or N-terminus of monomer peptides with introduction of 2 or 3 Glu–Lys pairs caused an efficient increase in the α-helicity of HR2 peptides. Taken together, our data show that dimerization at the C-terminus is superior to dimerization at the N-terminus in case of HR2 peptide derivatives endowed with relatively high potency. Dimer **3C** and **4C** were the most suitable derivatives. In the present study, VeroE6 cells were used for plaque reduction assays, and living cells can be clearly observed 2 days after treatment with the synthesized HR2 peptides at concentrations below 100 μM. This suggests that these peptides might not have significant cytotoxicity, although precise investigation on cytotoxicity is required.

In our previous study on HIV-1 fusion inhibitors, the C-terminal dimer of the HIV-1 HR2 region peptide has significantly more potent antiviral activity than the N-terminal dimer and the corresponding monomer peptide.[27] This phenomenon was also observed with SARS-CoV-2. It is confirmed that the C-terminal dimerization strategy might be useful for the design of inhibitors against viruses with fusion mechanism involving HR1-HR2 interactions.[8,9,15,20–23] The obtained dimers (**3C** and **4C**) are useful leads for antiviral agents for therapy of COVID-19. To date, new corona virus-caused infectious diseases, including SARS[29,30] and middle east respiratory syndrome (MERS)[39] have been repeated. Although COVID-19 may be stamped out, expansion of new infectious diseases caused by different corona viruses might be possibly of concern. Therefore, it is possible to apply the present strategy to the design of inhibitors against these diseases.

# Experimental section

### Compound synthesis

All materials and methods including general information, details of synthesis and characterization of the compounds are available in the ESI.† The synthetic methods for compounds are described in Schemes 1–4. The purity of the final compounds as measured by analytical HPLC was >95%.

### Antiviral assay (plaque reduction assay)

One hundred plaque-forming units of SARS-CoV-2 (OMC-510)[37] were mixed with peptides (or DMSO) in 200 μL of Dulbecco's Modified Eagle's Medium and the mixture was subjected to plaque-forming assays. VeroE6/TMPRSS2 cells[35] were seeded in 24-well plates ($1.5 \times 10^5$ cells per well) at 1 day before the assay and incubated with the virus/peptide mixture at 37 °C for 2 h. After removal of the mixture, cells were cultured with Eagle's minimum essential medium containing 1% methylcellulose 4000 cp (Fujifilm, Wako Pure Chemical Corporation, Japan) and 2% fetal bovine serum. Two days after infection, the cells were fixed with formaldehyde. Then, the plaques were visualized by staining with 1% crystal violet and counted.

### CD spectroscopy

CD measurements were performed with a J-720 circular dichroism spectropolarimeter equipped with a thermo-regulator (JASCO, Japan). The wavelength dependence of molar ellipticity [$\theta$] at 25 °C was monitored from 200 to 250 nm. The peptides were dissolved in PBS (50 mM sodium phosphate, 150 mM NaCl, pH 7.2) and measured at a concentration of 100 μM with the exception of peptides **1N** (25 μM), **4a** (50 μM) and **4C** (50 μM). The spectral data were corrected by Spectra Manager v1.54.03 [Build 1] (JASCO) and analyzed by Microsoft Excel, and the Figure was prepared by GraphPad Prism 9.

# Author contributions

Conceptualization, K. T. and H. T.; methodology, K. T. and Y. S.; validation, K. T. and Y. S.; formal analysis, K. T. and K. O.; investigation, K. T., K. O., Y. M, T. I., K. S., T. K. and A. E.; writing—original draft preparation, K. T.; writing—review and editing, H. T.; supervision, Y. S., T. N. and H. T. All authors have read and agreed to the published version of the manuscript.

# Conflicts of interest

The authors declare that they have no known competing financial interests or personal relationships that could have appeared to influence the work reported in this paper.

# Acknowledgements

The authors deeply thank Dr Ryo Masuda and Prof. Takaki Koide (Waseda Univ.) for measuring CD spectra. This work was supported in part by JSPS KAKENHI Grant Numbers 20H03362 (H. T.) and 22K15243 (K. T.); Research Program on HIV/AIDS, Japan

Agency for Medical Research and Development (AMED) JP21am0101098 and JP22ama121043 (Platform Project for Supporting Drug Discovery and Life Science Research, BINDS) (H. T.). This study was also supported financially by the research grant of Astellas Foundation for Research on Metabolic Disorders and Chugai Foundation for Innovative Drug Discovery Science: C-FINDs (K. T.). This research is based on the Cooperative Research Project of Research Center for Biomedical Engineering.

## Notes and references

1 World Health Organization, *COVID-19 vaccine tracker and landscape*, **https://www.who.int/publications/m/item/draft-landscape-of-covid-19-candidate-vaccines**, accessed on 2022-7-6.

2 J. Pardo, A. M. Shukla, G. Chamarthi and A. Gupte, *Drugs Context*, 2020, **9**, DOI: **10.7573/dic.2020-4-14**.

3 U.S. Food & Drug Administration, *FDA approves first treatment for COVID-19*, **https://www.fda.gov/news-events/pressannouncements/fda-approves-first-treatment-covid-19**, accessed on 2021-1-21.

4 *Merck and Ridgeback's Investigational Oral Antiviral Molnupiravir Reduced the Risk of Hospitalization or Death by Approximately 50% Compared to Placebo for Patients with Mild or Moderate COVID-19 in Positive Interim Analysis of Phase 3 Study*, Press Release from Merck & Co., Inc., 2021, accessed on 2022-5-12.

5 World Health Organization, WHO updates its treatment guidelines to include molnupiravir, March 3, 2022, **https://www.who.int/news/item/03-03-2022-molnupiravir**, accessed on 2022-5-12.

6 J. A. McIntosh, T. Benkovics, S. M. Silverman, M. A. Huffman, J. Kong, P. E. Maligres, T. Itoh, H. Yang, D. Verma, W. Pan, H.-I. Ho, J. Vroom, A. M. Knight, J. A. Hurtak, A. Klapars, A. Fryszkowska, W. J. Morris, N. A. Strotman, G. S. Murphy, K. M. Maloney and P. S. Fier, *ACS Cent. Sci.*, 2021, **7**, 1980–1985.

7 D. R. Owen, C. M. N. Allerton, A. S. Anderson, L. Aschenbrenner, M. Avery, S. Berritt, B. Boras, R. D. Cardin, A. Carlo, K. J. Coffman, A. Dantonio, L. Di, H. Eng, R. Ferre, K. S. Gajiwala, S. A. Gibson, S. E. Greasley, B. L. Hurst, E. P. Kadar, A. S. Kalgutkar, J. C. Lee, J. Lee, W. Liu, S. W. Mason, S. Noell, J. J. Novak, R. S. Obach, K. Ogilvie, N. C. Patel, M. Pettersson, D. K. Rai, M. R. Reese, M. F. Sammons, J. G. Sathish, R. S. P. Singh, C. M. Steppan, A. E. Stewart, J. B. Tuttle, L. Updyke, P. R. Verhoest, L. Wei, Q. Yang and Y. Zhu, *Science*, 2021, **374**, 1586–1593.

8 T. Tang, M. Bidon, J. A. Jaimes, G. R. Whittaker and S. Daniela, *Antivir. Res.*, 2020, **178**, 104792.

9 C. B. Jackson, M. Farzan, B. Chen and H. Choe, *Nat. Rev. Mol. Cell Biol.*, 2022, **23**, 3–20.

10 Y. Zhu, D. Yu, H. Yan, H. Chong and Y. He, *J. Virol.*, 2020, **94**, e00635-20.

11 D. Yu, Y. Zhu, T. Jiao, T. Wu, X. Xiao, B. Qin, H. Chong, X. Lei, L. Ren, S. Cui, J. Wang and Y. He, *Emerg. Microbes Infect.*, 2021, **10**, 1227–1240.

12 M. Zheng, W. Cong, H. Peng, J. Qing, H. Shen, Y. Tang, C. Geng, S. Chen, Y. Zou, W.-D. Zhang, H.-G. Hu and X. Li, *J. Med. Chem.*, 2021, **64**, 17486–17495.

13 A. Dahal, J. J. Sonju, K. G. Kousoulas and S. D. Jois, *J. Pept. Sci.*, 2022, **114**, e24245.

14 S. Xia, Y. Zhu, M. Liu, Q. Lan, W. Xu, Y. Wu, T. Ying, S. Liu, Z. Shi, S. Jiang and L. Lu, *Cell. Mol. Immunol.*, 2020, **17**, 765–767.

15 S. Xia, M. Liu, C. Wang, W. Xu, Q. Lan, S. Feng, F. Qi, L. Bao, L. Du, S. Liu, C. Qin, F. Sun, Z. Shi, Y. Zhu, S. Jiang and L. Lu, *Cell Res.*, 2020, **30**, 343–355.

16 V. Papanikolaou, A. Chrysovergis, V. Ragos, E. Tsiambas, S. Katsinis, A. Manoli, S. Papouliakos, D. Roukas, S. Mastronikolis, D. Peschos, A. Batistatou, E. Kyrodimos and N. Mastronikolis, *Gene*, 2022, **814**, 146134.

17 E. Takashita, N. Kinoshita, S. Yamayoshi, Y. Sakai-Tagawa, S. Fujisaki, M. Ito, K. Iwatsuki-Horimoto, P. Halfmann, S. Watanabe, K. Maeda, M. Imai, H. Mitsuya, N. Ohmagari, M. Takeda, H. Hasegawa and Y. Kawaoka, *N. Engl. J. Med.*, 2022, **386**, 1475–1477.

18 Y. Cao, A. Yisimayi, F. Jian, W. Song, T. Xiao, L. Wang, S. Du, J. Wang, Q. Li, X. Chen, Y. Yu, P. Wang, Z. Zhang, P. Liu, R. An, X. Hao, Y. Wang, J. Wang, R. Feng, H. Sun, L. Zhao, W. Zhang, D. Zhao, J. Zheng, L. Yu, C. Li, N. Zhang, R. Wang, X. Niu, S. Yang, X. Song, Y. Chai, Y. Hu, Y. Shi, L. Zheng, Z. Li, Q. Gu, F. Shao, W. Huang, R. Jin, Z. Shen, Y. Wang, X. Wang, J. Xiao and X. S. Xie, *Nature*, 2022, **608**, 593–602.

19 Q. Wang, Y. Guo, S. Iketani, M. S. Nair, Z. Li, H. Mohri, M. Wang, J. Yu, A. D. Bowen, J. Y. Chang, J. G. Shah, N. Nguyen, Z. Chen, K. Meyers, M. T. Yin, M. E. Sobieszczyk, Z. Sheng, Y. Huang, L. Liu and D. D. Ho, *Nature*, 2022, **608**, 603–608.

20 H. Tamamura, T. Kobayakawa and N. Ohashi, *Springer Briefs in Pharmaceutical Science & Drug Development*, Springer, Singapore, 2018, pp. 1—100.

21 E. O. Freed and M. A. Martin, *J. Biol. Chem.*, 1995, **270**, 23883–23886.

22 R. Wyatt and J. Sodroski, *Science*, 1998, **280**, 1884–1888.

23 D. M. Eckert and P. S. Kim, *Annu. Rev. Biochem.*, 2001, **70**, 777–810.

24 A. Otaka, M. Nakamura, D. Nameki, E. Kodama, S. Uchiyama, S. Nakamura, H. Nakano, H. Tamamura, Y. Kobayashi, M. Matsuoka and N. Fujii, *Angew. Chem., Int. Ed.*, 2002, **41**, 2937–2940.

25 W. Nomura, C. Hashimoto, A. Ohya, K. Miyauchi, E. Urano, T. Tanaka, T. Narumi, T. Nakahara, J. A. Komano, N. Yamamoto and H. Tamamura, *ChemMedChem*, 2012, **7**, 205–208.

26 W. Nomura, C. Hashimoto, T. Suzuki, N. Ohashi, M. Fujino, T. Murakami, N. Yamamoto and H. Tamamura, *Bioorg. Med. Chem.*, 2013, **21**, 4452–4458.

27 T. Kobayakawa, K. Ebihara, Y. Honda, M. Fujino, W. Nomura, N. Yamamoto, T. Murakami and H. Tamamura, *ChemBioChem*, 2019, **20**, 2101–2108.

28 T. Kobayakawa, K. Ebihara, K. Tsuji, T. Kawada, M. Fujino, Y. Honda, N. Ohashi, T. Murakami and H. Tamamura, *Bioorg. Med. Chem.*, 2020, **28**, 115812.
29 World Health Organization, *Severe Acute Respiratory Syndrome (SARS)*, **https://www.who.int/health-topics/severe-acute-respiratory-syndrome#tab=tab_1**, accessed on 2022-7-6.
30 U. D. Parashar and L. J. Anderson, *Int. J. Epidemiol.*, 2004, **33**, 628–634.
31 M. Ujike, H. Nishikawa, A. Otaka, N. Yamamoto, N. Yamamoto, M. Matsuoka, E. Kodama, N. Fujii and F. Taguchi, *J. Virol.*, 2008, **82**, 588–592.
32 W. Nomura, C. Hashimoto, A. Ohya, K. Miyauchi, E. Urano, T. Tanaka, T. Narumi, T. Nakahara, J. A. Komano, N. Yamamoto and H. Tamamura, *ChemMedChem*, 2012, **7**, 205–208.
33 S. Futaki, T. Suzuki, W. Ohashi, T. Yagami, S. Tanaka, K. Ueda and Y. Sugiura, *J. Biol. Chem.*, 2001, **276**, 5836–5840.
34 M. Hoffmann, H. Kleine-Weber, S. Schroeder, N. Krüger, T. Herrler, S. Erichsen, T. S. Schiergens, G. Herrler, N.-H. Wu, A. Nitsche, M. A. Müller, C. Drosten and S. Pöhlmann, *Cell*, 2020, **181**, 271–280.
35 S. Matsuyama, N. Nao, K. Shirato, M. Kawase, S. Saito, I. Takayama, N. Nagata, T. Sekizuka, H. Katoh, F. Kato, M. Sakata, M. Tahara, S. Kutsuna, N. Ohmagari, M. Kuroda, T. Suzuki, T. Kageyama and M. Takeda, *Proc. Natl. Acad. Sci. U. S. A.*, 2020, **117**, 7001–7003.
36 P. E. Dawson, T. W. Muir, I. Clark-Lewis and S. B. Kent, *Science*, 1994, **266**, 776–779.
37 Y. Suzuki, T. Hishiki, A. Emi, S. Sakaguchi, R. Itamura, R. Yamamoto, T. Matsuzawa, K. Shimotohno, M. Mizokami, T. Nakano and N. Yamamoto, *Biochem. Biophys. Res. Commun.*, 2021, **575**, 36–41.
38 B. Meng, A. Abdullahi, I. A. T. M. Ferreira, N. Goonawardane, A. Saito, I. Kimura, D. Yamasoba, P. P. Gerber, S. Fatihi, S. Rathore, S. K. Zepeda, G. Papa, S. A. Kemp, T. Ikeda, M. Toyoda, T. S. Tan, J. Kuramochi, S. Mitsunaga, T. Ueno, K. Shirakawa, A. Takaori-Kondo, T. Brevini, D. L. Mallery, O. J. Charles, J. E. Bowen, A. Joshi, A. C. Walls, L. Jackson, D. Martin, K. G. C. Smith, J. Bradley, J. A. G. Briggs, J. Choi, E. Madissoon, K. B. Meyer, P. Mlcochova, L. Ceron-Gutierrez, R. Doffinger, S. A. Teichmann, A. J. Fisher, M. S. Pizzuto, A. de Marco, D. Corti, M. Hosmillo, J. H. Lee, L. C. James, L. Thukral, D. Veesler, A. Sigal, F. Sampaziotis, I. G. Goodfellow, N. J. Matheson, K. Sato and R. K. Gupta, CITIID-NIHR BioResource COVID-19 Collaboration; Genotype to Phenotype Japan (G2P-Japan) Consortium; Ecuador-COVID19 Consortium, *Nature*, 2022, **603**, 706–714.
39 World Health Organization, Middle East respiratory syndrome coronavirus (MERS-CoV) – update, May 31, 2013, **https://www.who.int/emergencies/disease-outbreak-news/item/2013_05_31_ncov-en**, accessed on 2022-7-20.